Impact of Deforestation on Regional Precipitation over the Indochina Peninsula

SHINJIRO KANAE, TAIKAN OKI, AND KATUMI MUSIAKE

Institute of Industrial Science, The University of Tokyo, Tokyo, Japan

(Manuscript received 8 November 1999, in final form 28 August 2000)

ABSTRACT

It is now widely recognized that tropical deforestation can change the regional climate significantly. The increasing population and the spreading deforestation in the Indochina Peninsula, especially in Thailand, make it urgent to assess the effects of deforestation on the regional climate. Most of the previous numerical experiments generally have shown that decreases in precipitation occur as a result of deforestation. However, in most cases, these hydrometeorological changes have not been detected in observations. In this study, the nonparametric Mann–Kendall rank test and linear regression analysis were applied to analyze precipitation data obtained over a period of more than 40 yr, for each month, at each meteorological station in Thailand. Significant decreases in precipitation over Thailand were detected only in the time series of monthly precipitation in September. Amounts of precipitation recorded at many meteorological stations in September have decreased by approximately 100 mm month^{-1} (approximately 30% relative change) over the past three or four decades. Numerical experiments with a regional climate model based on the Regional Atmospheric Modeling System with a simple land surface scheme were carried out for the Indochina Peninsula. In these experiments, the type of vegetation in the northeastern part of Thailand was specified as either short vegetation (the current vegetation type) or forest (the former vegetation type). The experiments were carried out using the initial and boundary meteorological conditions of August and September in 1992–94. The initial and boundary conditions were interpolated from the data of the National Centers for Environmental Prediction–National Center for Atmospheric Research reanalysis. In these numerical experiments, a decrease in precipitation over the deforested area was obtained for September, but not for August. The magnitude of the mean decrease in precipitation over the whole deforested area in these experiments was 26 mm month^{-1} (7% relative change), and the local maximum decrease was 88 mm month^{-1} (29% relative change). Precipitation in the wet season over the Indochina Peninsula basically occurs under the influence of the Southeast Asian summer monsoon system. The strong summer monsoon westerlies bring abundant moisture to the Indochina Peninsula as a source of precipitation. The monsoon westerlies are the predominant external force influencing the regional climate. However, the strong westerlies over the Indochina Peninsula disappear in September, although that is typically the month of maximum precipitation. Accordingly, it is inferred that the effect of local deforestation appears significantly only in September because of the absence of this strong external force.

1. Introduction

The impact of tropical deforestation on climate has been a controversial issue because possible climate changes induced by deforestation may affect society and the world's most diverse ecosystem in the Tropics. Although it has been gradually accepted that the land surface and terrestrial ecosystems are influential components of the global climate system (Pielke et al. 1998), the impact of deforestation on climate is not yet well understood (Gash and Nobre 1997). Therefore, adequate scientific assessment is indispensable. Although tropical deforestation could change the global climate (Chase et al. 1996), changes in regional hydrological cycles (e.g.,

Henderson-Sellers et al. 1993; Zheng and Eltahir 1998) have been recognized as one of the major subject areas to be addressed.

Several numerical experiments on deforestation were carried out (e.g., Henderson-Sellers and Gornitz 1984; Dickinson and Henderson-Sellers 1988; Sud et al. 1996; Lean and Rowntree 1997), focusing on the Amazonian deforestation. In most cases, these experiments showed a decrease in precipitation as a result of deforestation. However, the predicted decrease in precipitation has not been detected clearly in observations. Chu et al. (1994) tried to examine a change in outgoing longwave radiation (OLR) over the Amazon basin, but no significant change supporting the results obtained in the numerical experiments was detected.

Numerical experiments examining the response to separate changes in roughness length and albedo have been conducted in several studies on the Amazonian deforestation (e.g., Hahmann and Dickinson 1997; Lean

Corresponding author address: Shinjiro Kanae, Institute of Industrial Science, The University of Tokyo, 4-6-1 Komaba, Meguro-ku, Tokyo 153-8505, Japan.
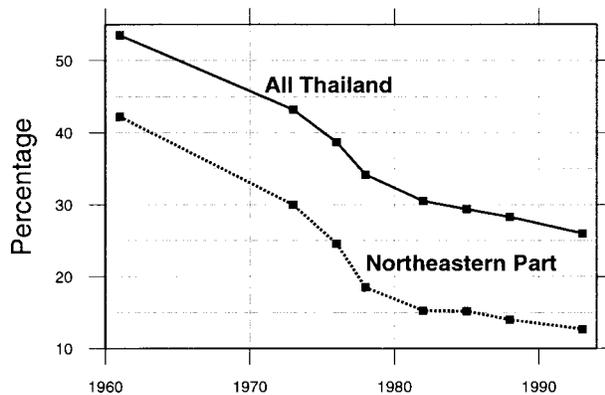E-mail: kanae@iis.u-Tokyo.ac.jp

FIG. 1. Time series of forested area in Thailand. Data source: Forestry Statistics of Thailand (Royal Forestry Department of Thailand).

and Rowntree 1997), prior to examining separate changes in other parameters, because an increase in albedo and a decrease in roughness length are considered to be major factors involved in deforestation effects on climate. An increase in albedo produces a decrease in downward shortwave radiation absorbed at the surface, which leads to a decrease in net radiation. The decrease in net radiation resulted in a decrease in evaporation in these studies. These decreases in net radiation and evaporation may cause a decrease in precipitation that is, however, uncertain because it is known that changes in moisture convergence, as well as decreases in net radiation and evaporation, contribute to changes in precipitation. The decrease in roughness length can produce a decrease in evaporation through a decrease in the surface drag coefficient (e.g., Hahmann and Dickinson 1997). The decrease in roughness length also produces a large change in the low-level wind field, which leads to a change in the moisture convergence. Therefore, the change in precipitation by the decrease in roughness length is complex and can vary from region to region. Thus, total deforestation, including both albedo and roughness changes, can produce a decrease in evaporation and complex changes in moisture convergence and precipitation.

Apart from the studies on Amazonian deforestation, there have been several other studies concerning precipitation changes due to anthropogenic landscape changes. The role of vegetation over West Africa has been examined in several studies (e.g., Xue and Shukla 1993; Zheng and Eltahir 1998). It was argued that deforestation or desertification is likely to be a significant contributor to the observed drought in West Africa. Pielke et al. (1999) carried out regional numerical experiments, for two months in summer, based on the 1900 landscape and the 1993 landscape in southern Florida. They obtained an 11% decrease in rainfall with the 1993 landscape, as compared with the simulation results with the 1900 landscape. They argued that the trends in summer rainfall as suggested by the limited available observations are consistent with the trends in the numerical

experiments. Unfortunately, records of observed rainfall were only available at three stations located at the coast or the shore. Because effects of anthropogenic landscape changes on regional climate should vary from region to region, studies on other regions are needed.

Although the Indochina Peninsula has been oppressed by the increasing population and the marked deforestation, only a few studies (e.g., Henderson-Sellers et al. 1993) have examined the effect of deforestation on the climate and the water resources over the peninsula. A time series of the percentage of forested land in Thailand [data from the Royal Forest Department of Thailand (1994)] is shown in Fig. 1. Thailand, a major part of the Indochina Peninsula, was highly forested in the past, but is not currently highly forested.

Some studies have examined a trend in precipitation (or OLR) over the Indochina Peninsula. Chu and Wang (1997) examined OLR over 22.5°N–22.5°S and 40°E–180° from 1974 to 1992. They found an increase in convection during the boreal summer (from April to September) from the Arabian Sea across Southeast Asia to the northwest Pacific. Watanabe and Shinoda (1996) analyzed the trend in observed precipitation in South and Southeast Asia and found a decrease from June through September over the western part of the Indochina Peninsula. The findings in these two studies do not match, even in terms of the signs of the trends. One possible reason for this discrepancy could be that Chu and Wang (1997) utilized coarse OLR data at a 5° resolution. Another reason could be that Watanabe and Shinoda (1996) referred to only the western part of the Indochina Peninsula. In addition, main subjects of interest in these studies were large-scale climatic change and variability related to sea surface temperature effects on climate, and little attention was paid to the effect of the regional land surface on climate.

Because observed precipitation data from 1951 to 1994 in Thailand are available, it is possible to identify the effect of deforestation on the regional climate through analysis of these data. However, the additional analysis of the effect on Cambodia and Laos, two neighboring regions belonging to the same climatic regime as Thailand, is difficult because of data availability.

The aim of this work is to determine the trend in the observed precipitation data and compare it with the results of numerical deforestation experiments. The basic climatology over the Indochina Peninsula is described in section 2 to allow better interpretation of the changes in precipitation. The trend in precipitation over Thailand for approximately the last 40 years is analyzed in section 3. Numerical experiments on deforestation using a regional climate model are described in section 4, and the results from these experiments are shown in section 5. A discussion and conclusions are provided in section 6.

2. Climate over Thailand

a. Data

Data used in this section and the next sections are observed precipitation data in Thailand (see below), the

National Centers for Environmental Prediction–National Center for Atmospheric Research (NCEP–NCAR) 40-Year Reanalysis (Kalnay et al. 1996), and the Global Precipitation Climatology Project (GPCP) dataset (Huffman et al. 1997). Daily precipitation data in the period from 1951 to 1994 were provided by the Thai Meteorological Department (TMD) and were summed up to monthly values. Because the climatological characteristics over the Malay Peninsula are very different from those of the mainland in Thailand, precipitation data observed in the mainland were adopted for the analysis. The locations of the observation stations are shown on the map in Fig. 6, which is described in section 3. The total number of the observation stations is 34. Precipitation data obtained at 26 out of 34 stations are available for 1951–94. Precipitation data obtained at the other 8 stations are available from 1952 (2 stations), 1953 (1 station), 1954 (3 stations), 1956 (1 station), and 1960 (1 station).

The NCEP–NCAR reanalysis was used to examine the large-scale climatological aspects of the Southeast Asian summer monsoon (SEAM). The NCEP–NCAR reanalysis was provided on a global $2.5° \times 2.5°$ grid system, and the data used in the climatological analysis are monthly mean data averaged over 1979–95. The reanalysis data at 850 hPa were used to represent the characteristics of the SEAM, and the data below 300 hPa were used for the calculation of atmospheric water vapor convergence. In the calculation of atmospheric water vapor convergence, not only the monthly mean wind velocity and specific humidity but also the covariances between wind velocity and specific humidity were utilized. Global monthly mean precipitation data by GPCP compiled both from observed precipitation data and satellite data was used in the calculation of atmospheric water vapor convergence, because the GPCP precipitation data are closer to the real amount of precipitation than are the precipitation data of the reanalysis, which are solely dependent on a climate model. Additionally the precipitation data from TMD do not cover the whole Indochina Peninsula, whereas the atmospheric water vapor convergence calculated on the basis of the NCEP–NCAR reanalysis covers a larger area than the whole Indochina Peninsula, because of the resolution of the reanalysis.

b. Characteristics of the climate over Thailand

In this subsection, the climate over Thailand and the Indochina Peninsula is briefly reviewed. Figure 2 shows the seasonal evolution of climatological monthly precipitation as measured at selected meteorological stations in Thailand. Switching between wet and dry seasons is predominant over the Indochina Peninsula as a part of the SEAM region. The onset of the wet season occurs in May, and its withdrawal occurs in October. The withdrawal of the wet season occurs in early October in the northern part of the Indochina Peninsula,
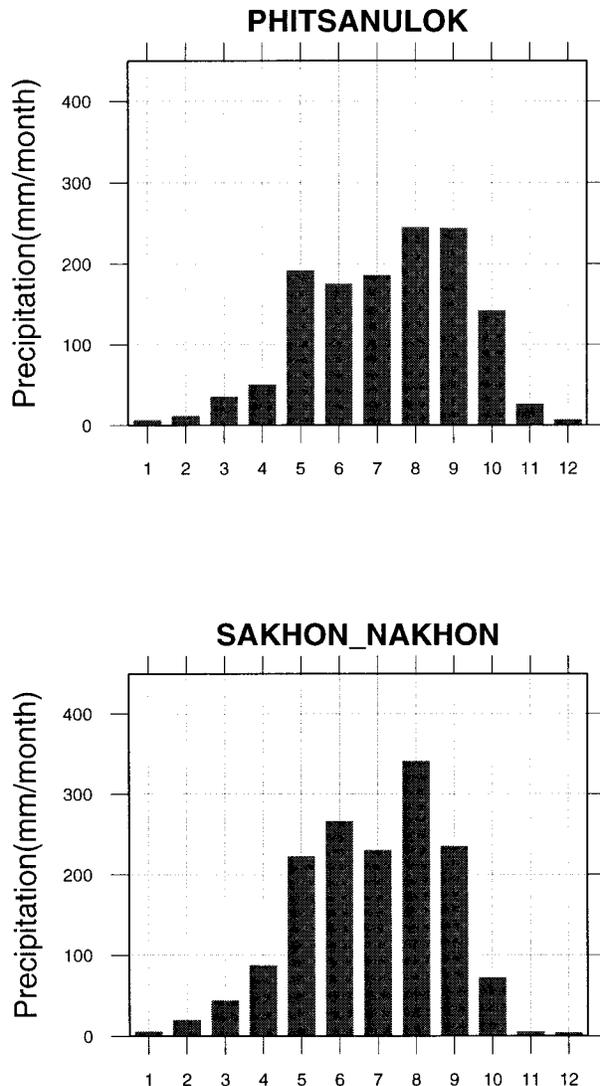

FIG. 2. Seasonal evolution of climatological monthly precipitation (mm month^{-1}) in Thailand, observed at Phitsanulok (16.78°N, 100.27°E) and Sakhon Nakhon (17.15°N, 104.13°E) averaged over 1951–94. The original data were provided by TMD.

in the central part of Thailand it occurs in the middle of October, and near Bangkok it occurs at the end of October.

Though it is not evident in these figures based on the monthly data, several additional characteristics were found in previous studies. Matsumoto (1995) pointed out that two peaks are clearly evident in the seasonal evolution of precipitation in Thailand, except at the northern edge of Thailand, if 5-day mean precipitation data are utilized for the analysis. One peak occurs in May and June, which is the beginning of the wet season. The other peak occurs in August and September, the final and mature stage of the wet season. These peaks occur because the zone of maximum precipitation over the Indochina Peninsula migrates northward in the be-
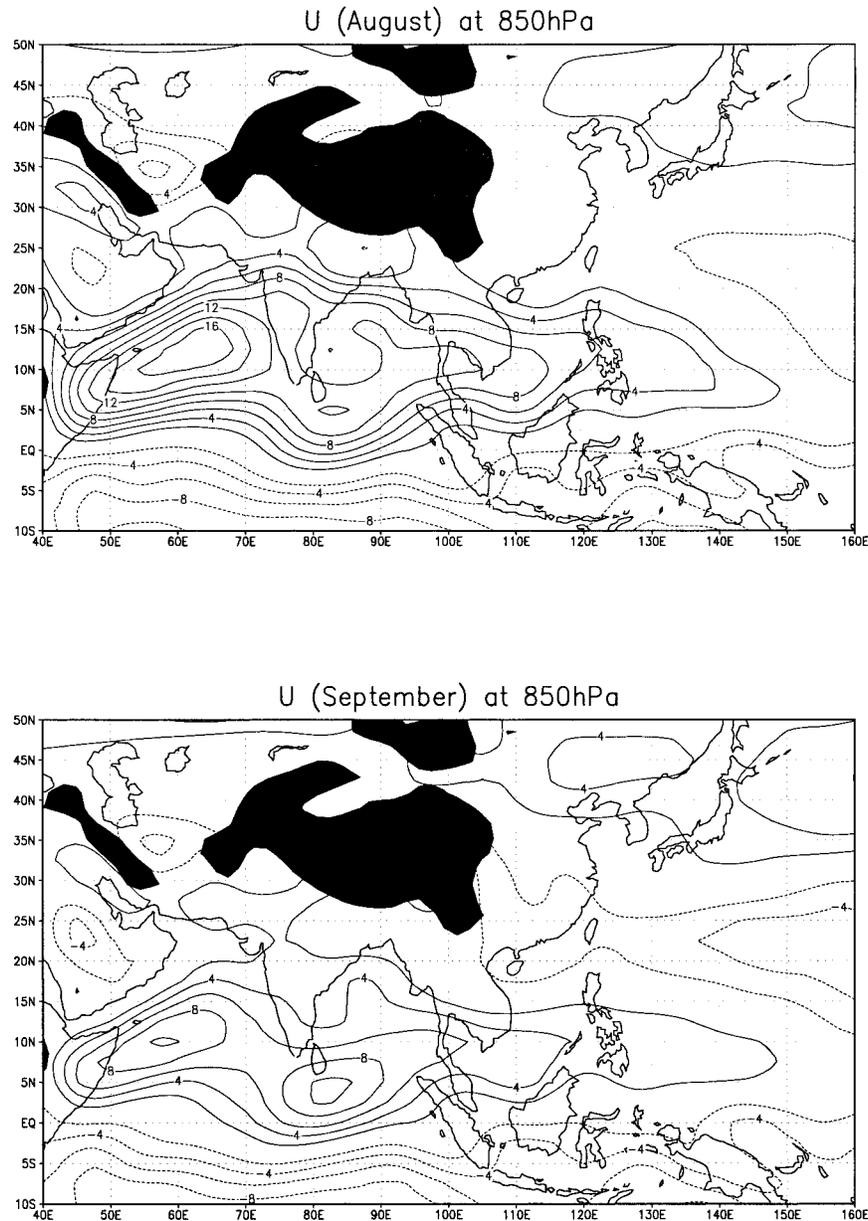
U (August) at 850hPa

U (September) at 850hPa

FIG. 3. Climatological zonal wind velocity (m s^{-1}) at 850 hPa over Asia in (top) Aug and (bottom) Sep based on the NCEP–NCAR reanalysis averaged over 1979–95.

ginning of the wet season and retreats southward in the withdrawal stage (Murakami and Matsumoto 1994). According to their research, the maximum precipitation zone is located around 5°N in May, moves to around 20°N at the end of July, then retreats southward, and reaches around 10°N in the middle of September.

As a background for the analysis in the following sections, the climate in the second peak of the wet season—August and September—is described below. The second peak of the wet season, both in August and September, occurs basically in the course of the retreat of the zone of maximum precipitation, as has been ex-

plained. However, the large-scale atmospheric circulation in August is different from that in September. Figure 3 shows the monthly mean zonal wind velocity at 850 hPa in August and September over Asia. In August, the strong monsoon westerlies, which bring abundant moisture as a source of precipitation, spread over the Arabian Sea, the Bay of Bengal, and the entire Indochina Peninsula. The monsoon westerlies at 850 hPa become generally weak in September. Figure 4 shows the seasonal changes in monthly mean zonal and meridional wind velocity at 850 hPa over the Indochina Peninsula. The disappearance of the summer monsoon westerlies over
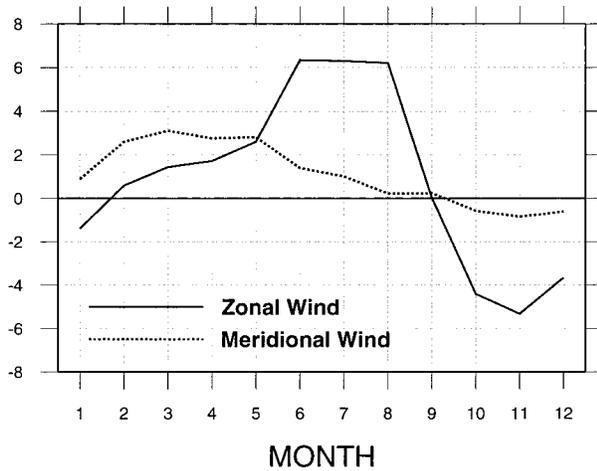
FIG. 4. Seasonal evolution in climatological zonal and meridional wind velocity (m s^{-1}) at 850 hPa over the Indochina Peninsula based on the NCEP–NCAR reanalysis averaged over 1979–95.

FIG. 5. Atmospheric water budget components over the Indochina Peninsula: water vapor flux convergence (mm month^{-1}), precipitation (mm month^{-1}), column storage of atmospheric water (mm), and evaporation (mm month^{-1}), based on the NCEP–NCAR reanalysis and the GPCP analysis.

the Indochina Peninsula can be detected in September. The term ''monsoon'' is generally defined as an annual reversal of wind direction between winter and summer (Khromov 1957) and sometimes has the meaning of distinct alternation between the wet and the dry season. However, the alternating period from the wet season to the dry season differs from the alternating period of wind direction in this case. In short, wind reverses before precipitation disappears.

To examine another aspect of the climate over the Indochina Peninsula, atmospheric water vapor convergence was calculated based on Oki et al. (1995). Atmospheric water balance is expressed as

$$-\nabla_H \cdot \mathbf{Q} = P - E + \frac{\partial W}{\partial t}, \qquad (1)$$

where $-\nabla_H \cdot \mathbf{Q}$, P, E, and W represent horizontal water vapor flux convergence, precipitation, evaporation, and total column storage of water substances (water vapor, cloud, and precipitating particles), respectively. In this equation, $-\nabla_H \cdot \mathbf{Q}$ and W were calculated from the NCEP–NCAR reanalysis, precipitation was provided by the GPCP data, and evaporation was calculated as a residual.

The atmospheric water balance over the Indochina Peninsula is shown in Fig. 5. Evaporation, the residual term, is examined to evaluate whether this water balance is reasonable. In the former studies (e.g., Jha et al. 1998), evaporation in the wet season was estimated to be approximately 4 mm day^{-1}. Thus the water balance estimation in the wet season in Fig. 5 is probably reasonable. On the other hand, the water balance in the dry season may have some defects, because evaporation has a negative value in a few months. In Fig. 5, no distinct difference is evident between the water balance in August and in September. The climate of atmospheric water balance is almost the same between August and Sep-
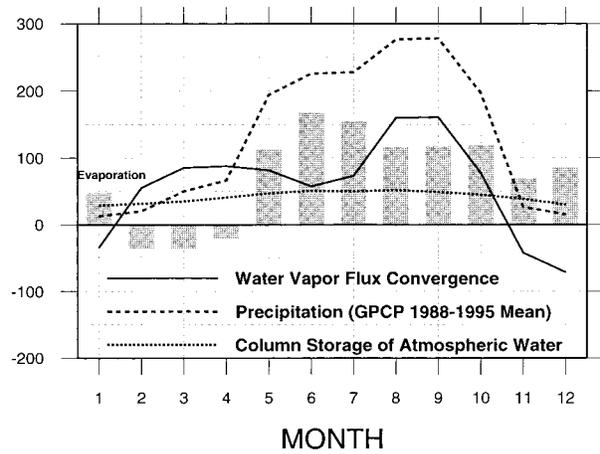
tember, although the vigor of the summer monsoon westerlies is different.

3. Trend in precipitation

The nonparametric Mann–Kendall rank test was carried out to detect the trend in precipitation for each month at each meteorological station in the period from 1951 to 1994. The Mann–Kendall rank τ was calculated following Kousky and Chu (1978); here, τ can be defined as a value between -1 and 1 when we have data points (x_i, y_i) $(i = 1, N)$, where N is the number of data points (Press et al. 1992). A positive (negative) estimate of τ indicates a positive (negative) trend. In the null hypothesis of no association between x_i and y_i, τ is approximately normally distributed, and the expectation value of τ is zero. The variance of τ is

$$\mathrm{Var}(\tau) = \frac{4N + 10}{9N(N - 1)}. \qquad (2)$$

Therefore, when the absolute value of the ratio of τ to its standard deviation is greater than 1.65, there is a significant correlation between x_i and y_i at the 90% level of confidence. In this case, x_i and y_i are year and precipitation, respectively. This test was applied at the 90% level of confidence. The nonparametric test was used because of the robustness and insensitiveness to the start and end points.

Another method, linear regression, was applied as well. The criteria described below were adopted for this analysis. At first, the trend (mm year^{-1}) was converted to the 50-yr trend. If the absolute value of this 50-yr trend was greater than 10% of the averaged monthly precipitation at each station, then this trend was accepted as a positive or a negative trend. This method was applied to detect the magnitude of the trend.

Results for each month in the wet season from May to October are shown in Fig. 6. The results obtained in the Mann–Kendall rank test are displayed with large stars (positive trends) and large triangles (negative trends) in the figure. A small mark indicates that the trend is statistically insignificant by the Mann–Kendall test, but a trend is evident by linear regression. Though the small marks are statistically insignificant in the Mann–Kendall test, we think they still provide some information, and for this reason they are displayed in the figure.

A few characteristics are found in Fig. 6. Significant negative trends are detected over almost all of Thailand in September; even the insignificant trends are mostly negative trends. Time series of precipitation at selected meteorological stations in September are shown in Fig. 7. Significant negative trends are evident in the figure. In addition, the magnitude of these negative trends in September is large as compared with that in other months. The magnitude of the decreases is approximately 100 mm month^{-1} (50 yr)$^{-1}$, which approximately corresponds to a relative change of 30%.

Another characteristic found in the trend analysis is the strong positive trends at a few stations at the northeastern edge of Thailand in July and August. These positive trends are displayed with large star marks on the middle panels of Fig. 6. The star marks at the northeastern edge of Thailand in July and August represent an increase of approximately 100–200 mm month^{-1} (50 yr)$^{-1}$. These characteristics are analyzed in the following sections.

4. Model and experiments

a. Model description

Numerical experiments were carried out in an effort to understand the decrease in precipitation in September. A regional climate model based on the Regional Atmospheric Modeling System (RAMS; Pielke et al. 1992) version 3b, developed at Colorado State University, was employed for these experiments. The basic equations were a set of nonhydrostatic compressive dynamic equations and a thermodynamic equation. Parameterizations of RAMS selected for physical processes included the following: 1) the Mellor–Yamada level-2.5 turbulence closure scheme (Mellor and Yamada 1982) for vertical diffusion, 2) a surface flux scheme based on Louis (1979), and 3) a cloud microphysics parameterization (Walko et al. 1995) to represent large-scale precipitation. In addition, several parameterizations below were incorporated into RAMS, as in Emori (1998). 4) a cumulus parameterization scheme based on Arakawa and Schubert (1974) with simplifications (Moorthi and Suarez 1992), and 5) a radiative transfer scheme with the k-distribution, two-stream discrete ordinate method based on Nakajima and Tanaka (1986).

A simplified land surface scheme was employed in this study. In the land surface scheme, surface temperature and ground temperature are calculated on the basis of the surface energy balance and multilayer diffusion. The scheme employed to calculate evaporation is the same as in Emori (1998), based on Manabe (1969), with a constant canopy resistance.

In this scheme, evaporation is calculated as follows:

$$E = \beta E_p = \beta \rho [q^*(T_w) - q_a]/(r_a + r_c), \qquad (3)$$

where E is evaporation, E_p is potential evaporation, β is evaporation efficiency, ρ is the density of air, q^* is saturated specific humidity, T_w is skin temperature, q_a is specific humidity of air, r_a is aerodynamic resistance, and r_c is a constant canopy resistance. Values of β were provided from one of the results of the Global Soil Wetness Project (GSWP; Dirmeyer et al. 1999). They were interpolated to the model grid points and fixed. The values of β used here were originally calculated in the GSWP using a land surface model that was a submodel of a general circulation model developed at the Center for Climate System Research (CCSR), The University of Tokyo, and named "LAND." The evaporation scheme of LAND is based on Manabe (1969) and is the same as in this study. Although no physiological effects are incorporated into this scheme, it validly produced hydrological components at the land surface, if compared with hydrological components produced by other land surface schemes (Dirmeyer et al. 1999; Oki et al. 1999) in the GSWP.

The land surface scheme in this study has two parameters, roughness length and albedo, that depend on vegetation type. Roughness length and albedo are major parameters of the land surface, which should be considered primarily in a deforestation simulation as described in the introduction. This simplicity of the land surface scheme makes it easy to analyze the simulation results and makes the mechanisms clear in the numerical experiments. That is why this simple scheme was used in this study. At the same time, the simple land surface scheme also has limitations. For instance, the changes in vegetation type at the surface do not only consist of changes in roughness length and albedo but also in changes in physiological effects. Despite its limitations, it was expected that meaningful results could be obtained within this framework.

b. Model setup and experimental design

The model domain shown in Fig. 8 has a 60-km grid spacing (50 × 50 grid points) horizontally and 25 layers vertically. Oblique polar stereo projection is employed, and the center of the domain is located at 14°N, 102°E. The topography is shown in Fig. 9. Mountain barriers on the west and the east borders of Thailand appear clearly with this resolution.

The periods of the experiments extend from 1 to 25 August and from 6 to 30 September (25 days in both cases) in 1992, 1993, and 1994. The experiments for
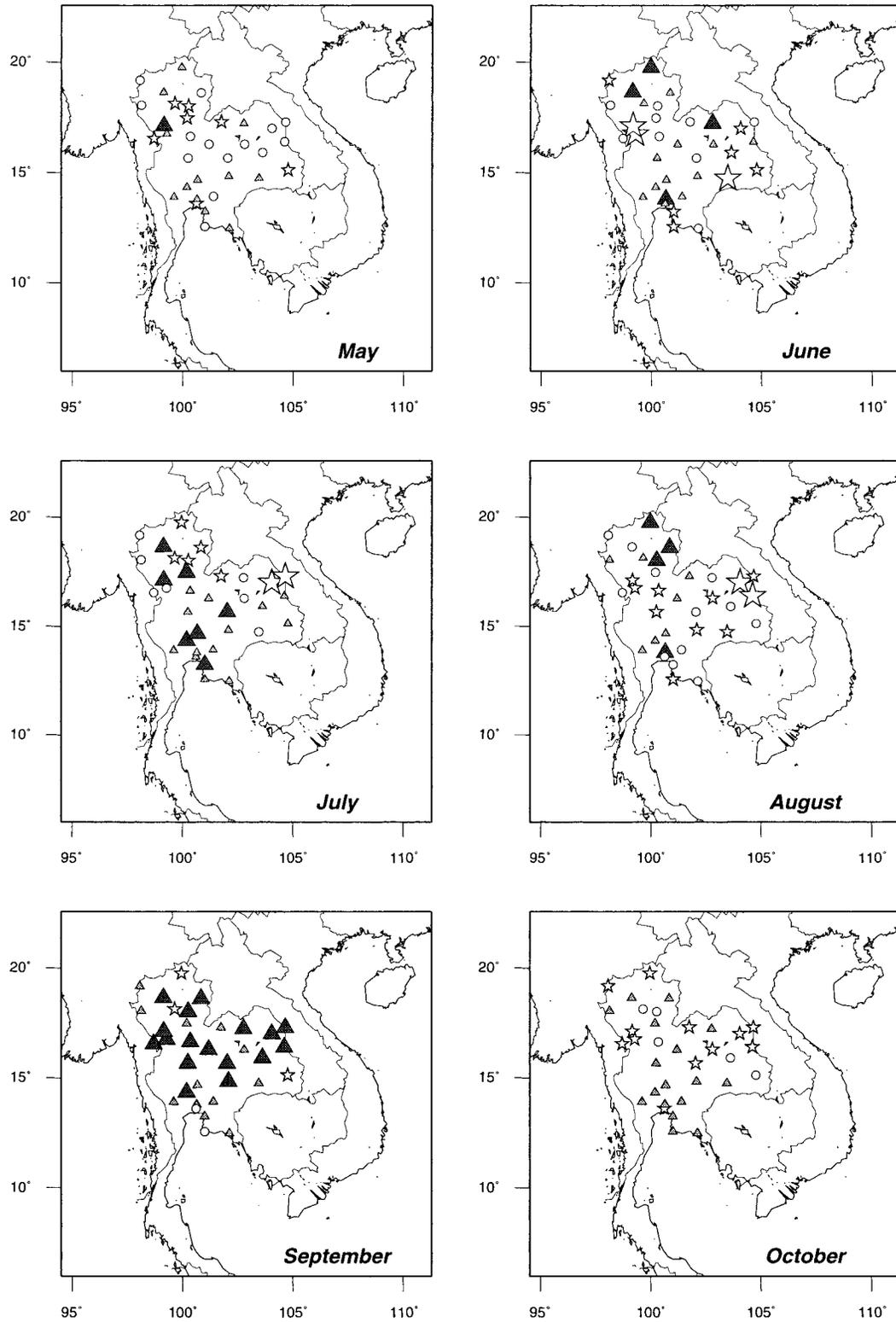
FIG. 6. Observed trend in precipitation in May, Jun, Jul, Aug, Sep, and Oct. A triangle indicates a negative trend, a star indicates a positive trend, and a circle indicates no trend. Large marks are statistically significant.
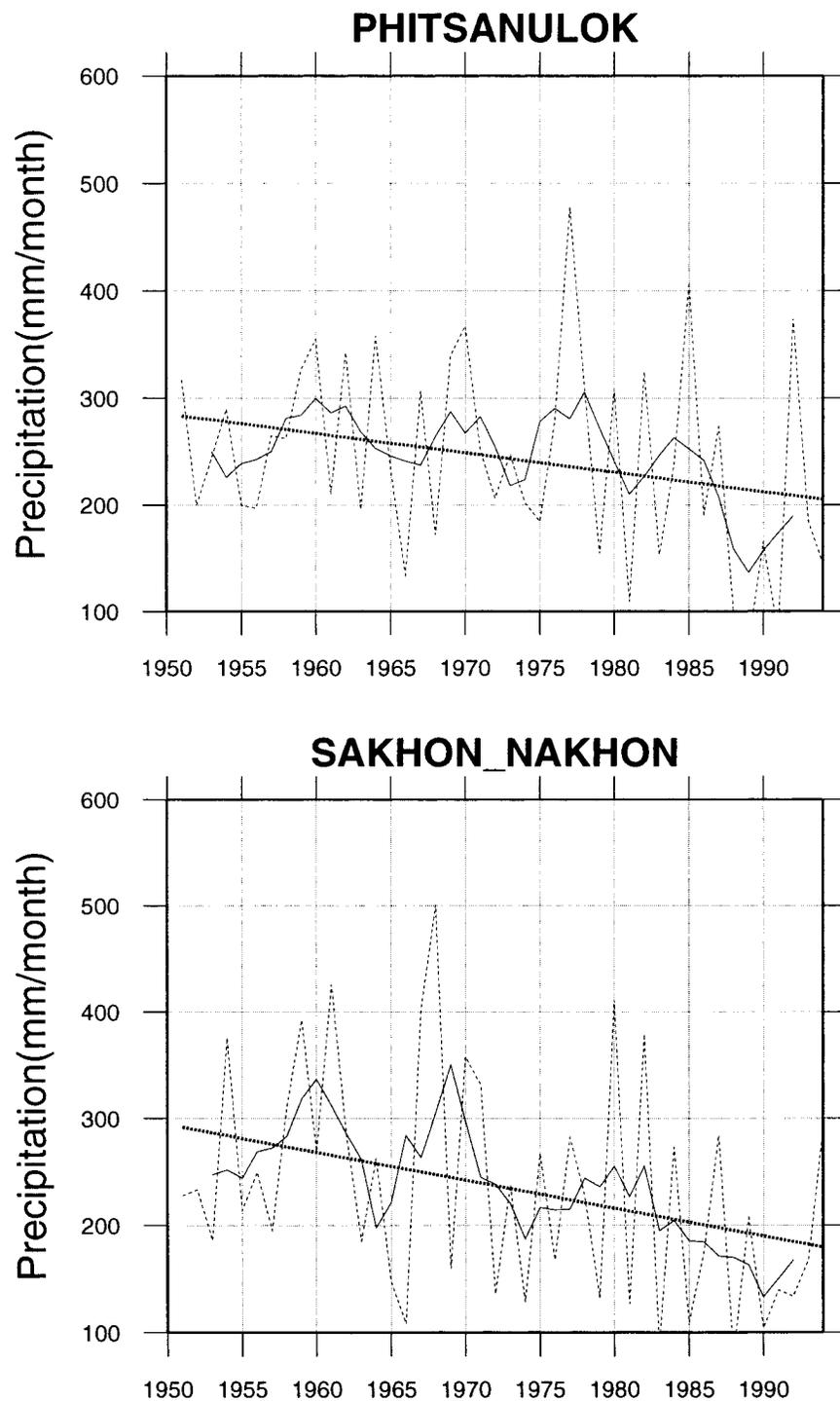
FIG. 7. Time series of precipitation (mm month^{-1}) observed at Phitsanulok (16.78°N, 100.27°E) and Sakhon Nakhon (17.15°N, 104.13°E) in Sep. The dashed line denotes annual values, the solid line denotes the 5-yr running mean, and the dotted line denotes the trend by linear regression. The original data were provided by TMD.
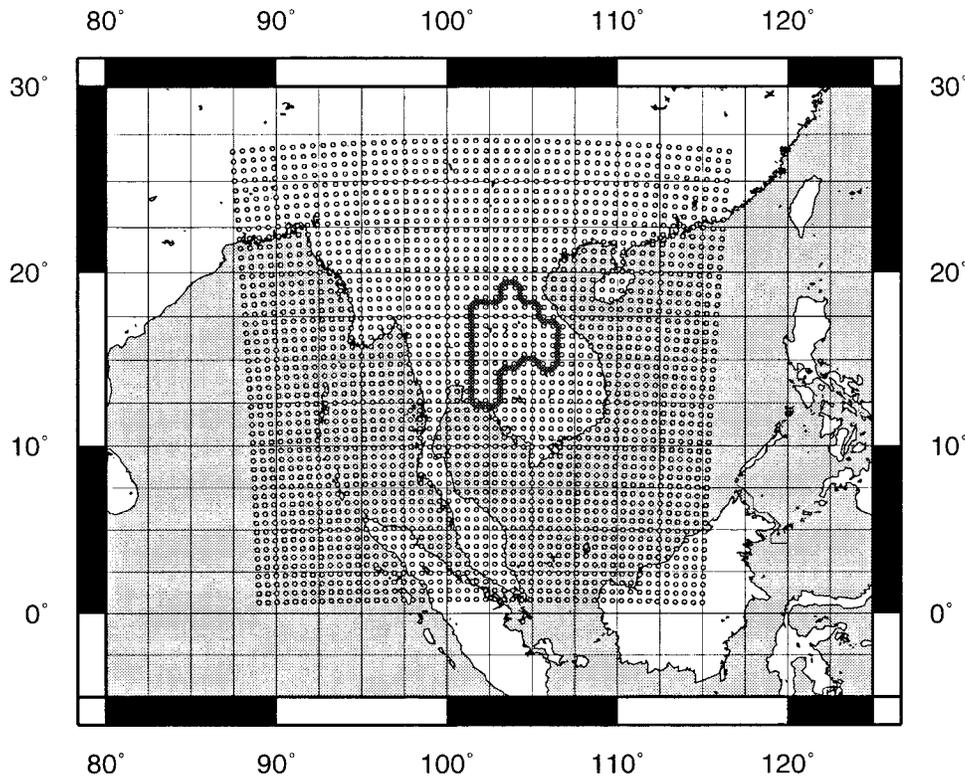
FIG. 8. Domain and horizontal grid distribution of the regional climate model. The thick line denotes ALSC in the model domain.

August and September were carried out separately, and the results obtained for the first 3 days were neglected in the following analysis to avoid the spinup problem. The simulation results shown in this report are averaged values for 22 days × 3 yr.

The meteorological initial and boundary conditions were interpolated from the NCEP–NCAR daily reanalysis. Davies relaxation (Davies 1976) lateral boundary

conditions were used at four grid points adjacent to each lateral boundary. Inside the model domain, basic prognostic variables were slightly nudged to the interpolated reanalysis to coincide with the large-scale climatic field.

The distribution of current vegetation in the model domain (Fig. 10) was specified from a set of global land surface parameters (Sellers et al. 1995), originally mapped on a 1° × 1° grid system based on satellite measurements. Albedo and roughness length for each vegetation type are shown in Table 1. They were determined as representative values for each vegetation type over Southeast Asia based on the set of global land surface parameters (Sellers et al. 1995). Because this set of global land surface parameters is one of the most comprehensive elaborate datasets, the distributions of vegetation type, albedo, and roughness length in the model domain should be reasonable.

The distribution of evaporation efficiency is shown in Fig. 11. The description of evaporation efficiency is provided in the preceding subsection. Sea surface temperatures were specified from a dataset of monthly mean values (Reynolds 1988). Numerical experiments with the distribution of current vegetation are labeled as "CRRT." CRRT represents the simulation after deforestation.

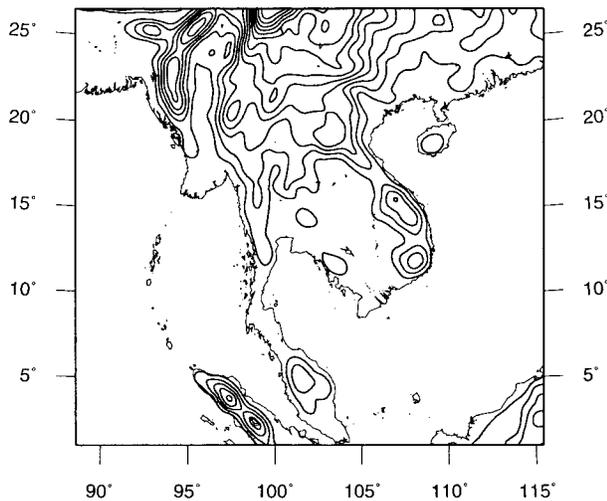Short vegetation (vegetation types 4 and 6) was changed to forest (vegetation type 1) at each grid point

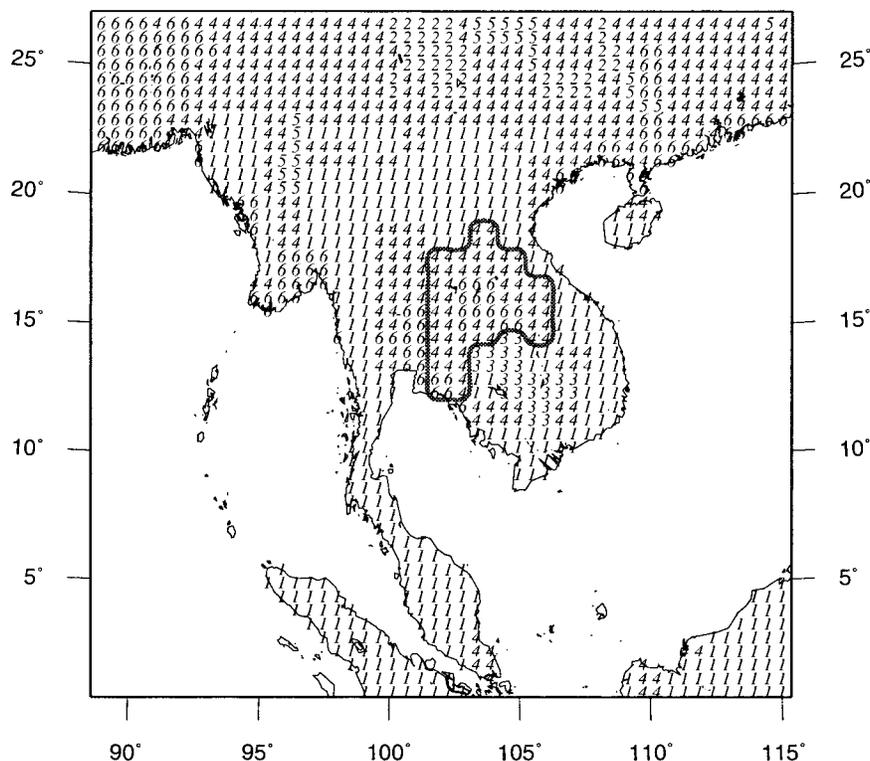FIG. 9. Topography in the model domain. Contour interval is 250 m.

FIG. 10. Distribution of vegetation type in the model domain, specified from a set of global land surface parameters (Sellers et al. 1995). The legend is given in Table 1. ALSC in the model domain is inside the thick line.

inside the thick line of Fig. 10 to represent the distribution of vegetation in the past. Vegetation types were changed only at the northeastern and the eastern part of Thailand, because these parts have been the most severely deforested areas in Thailand (Arbhabhirama et al. 1988), and because the central plain of Thailand had already been a developed area in the past, and the current percentage of the deforested area in the northern part is not large. Therefore, the vegetation types in the central part and the northern part were unchanged in the simulation. However, this distribution of vegetation in the past is somewhat imaginary, because the exact distribution of vegetation before deforestation is unknown and because actual deforestation tends to proceed as a subgrid-scale land surface alteration.

Numerical experiments with the distribution of vegetation in the past are labeled as "PAST." In the fol-

lowing, the area where the vegetation type was changed between CRRT and PAST is named the area of land surface change (ALSC).

The setup of evaporation efficiency β within ALSC in each experiment is shown in Table 2. Evaporation efficiency within ALSC was arbitrarily defined as $\beta = 1$ in PAST, because most evaporation efficiency values in forest covered areas in CRRT were 1.

Another set of experiments was carried out in which evaporation efficiency values in ALSC were the same as in CRRT, whereas the values of other parameters remained the same as in PAST. This set of experiments differs from CRRT in vegetation factors (albedo and roughness length) and is labeled "VEGT." These two contrastive settings—PAST and VEGT—differ only in terms of β and can help us to assess the effects of land surface changes with our simple land surface scheme.

5. Results of the numerical experiments

a. Validation of simulated precipitation

Simulated mean precipitation in August is compared with the GPCP analysis in August, as shown in the upper panels of Fig. 12. The amount of simulated precipitation averaged over the model domain is 7.6 mm day^{-1}, whereas the amount of precipitation over the same area, according to the GPCP analysis, is 7.4 mm day^{-1}.
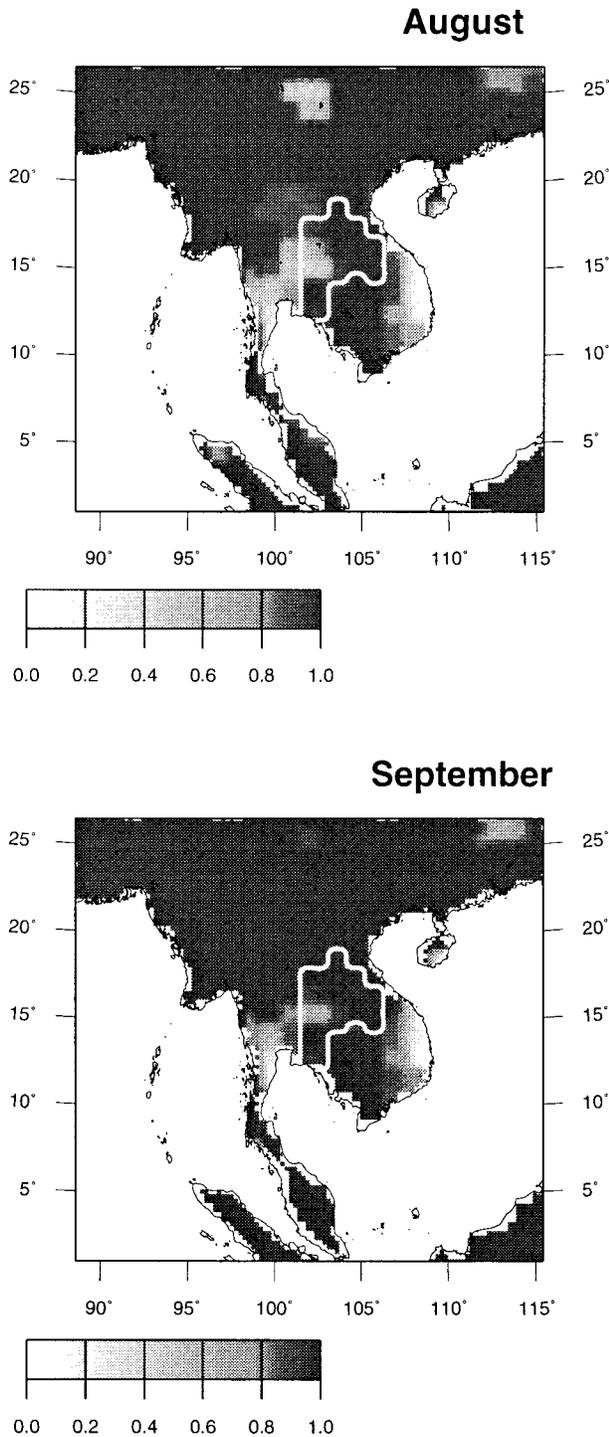
TABLE 1. Parameter values for each vegetation type.

No.	Vegetation type	Albedo	Roughness length (m)
1	Broadleaf evergreen forest	0.13	2.8
2	Mixed coniferous and broadleaf forest	0.10	1.0
3	Broadleaf deciduous forest and woodland	0.13	0.6
4	Wooded grassland	0.17	0.13
5	Grassland	0.18	0.12
6	Cultivation	0.16	0.12

August

TABLE 2. Evaporation efficiency and vegetation within ALSC in each experiment.

	CRRT	PAST	VEGT
Evaporation efficiency	–	$\beta = 1$	The same as in CRRT
Vegetation	Deforested	Forested	Forested

peaks of precipitation along the southwestern coasts in August were obtained in the simulation, approximately centered at 11°N, 103°E and 16°N, 98°E. These two peaks are considered to be reasonable, because the high mountains on the southwestern coasts in the Indochina Peninsula and the monsoon westerlies can lead to abundant precipitation on the windward side of the mountains. For instance, averaged over 1992–94, the amount of observed precipitation in August at Chamthaburi station at 12.6°N, 102.1°E on the southwestern coast is 20.5 mm day^{-1}, which approximately corresponds to the peak value near the station in the simulated result. A faint peak centered at 15°N, 106°E near the deforested area was obtained in the simulation, which is not evident in the GPCP analysis. This result is almost the same as the situation along the southwestern coasts described above.

Thus, the area mean precipitation was simulated fairly well, and the orography in the model domain led to a reasonable horizontal precipitation distribution. Almost the same characteristics are evident in the case of September, as shown in the lower panels of Fig. 12.

b. Change in precipitation over ALSC

Changes in some climate variables as a result of the numerical experiments on deforestation are presented in the following sections. Results of (CRRT − PAST) are introduced first. If the result of (CRRT − PAST) is a negative (positive) value, we will express it as a decrease (increase).

Changes in precipitation are shown in Fig. 13. A cross mark in this figure denotes significance at the 95% level as determined by the Student's t test. In August, a decrease in precipitation in the western part of ALSC and an increase in the eastern part of ALSC were simulated. The increase in simulated precipitation in the eastern part of ALSC in August may correspond to the observed increase in precipitation at the northeastern edge of Thailand. The maximum increase in observed precipitation in August in the northeastern part, measured at Sakon Nakhon station, is 190 mm month^{-1} (50 yr)$^{-1}$, which corresponds to 56% of the monthly mean precipitation at that station. The maximum increase in simulated precipitation in August at a grid point in the eastern part of ALSC is 134 mm month^{-1}, which corresponds to 24% of the mean simulated precipitation at that grid point.

On the other hand, in September, an overall decrease in precipitation over ALSC was obtained in the simu-

September

FIG. 11. Distribution of evaporation efficiency in (top) Aug and (bottom) Sep.

One of the major reasons for the difference between the distribution of simulated precipitation and the distribution of the GPCP analysis in August is the coarse grid spacing (2.5°) of the GPCP analysis. It makes a smooth field in the left panels of Fig. 12. Two notable

GPCP Rainfall (August)

Simulated Rainfall (August)

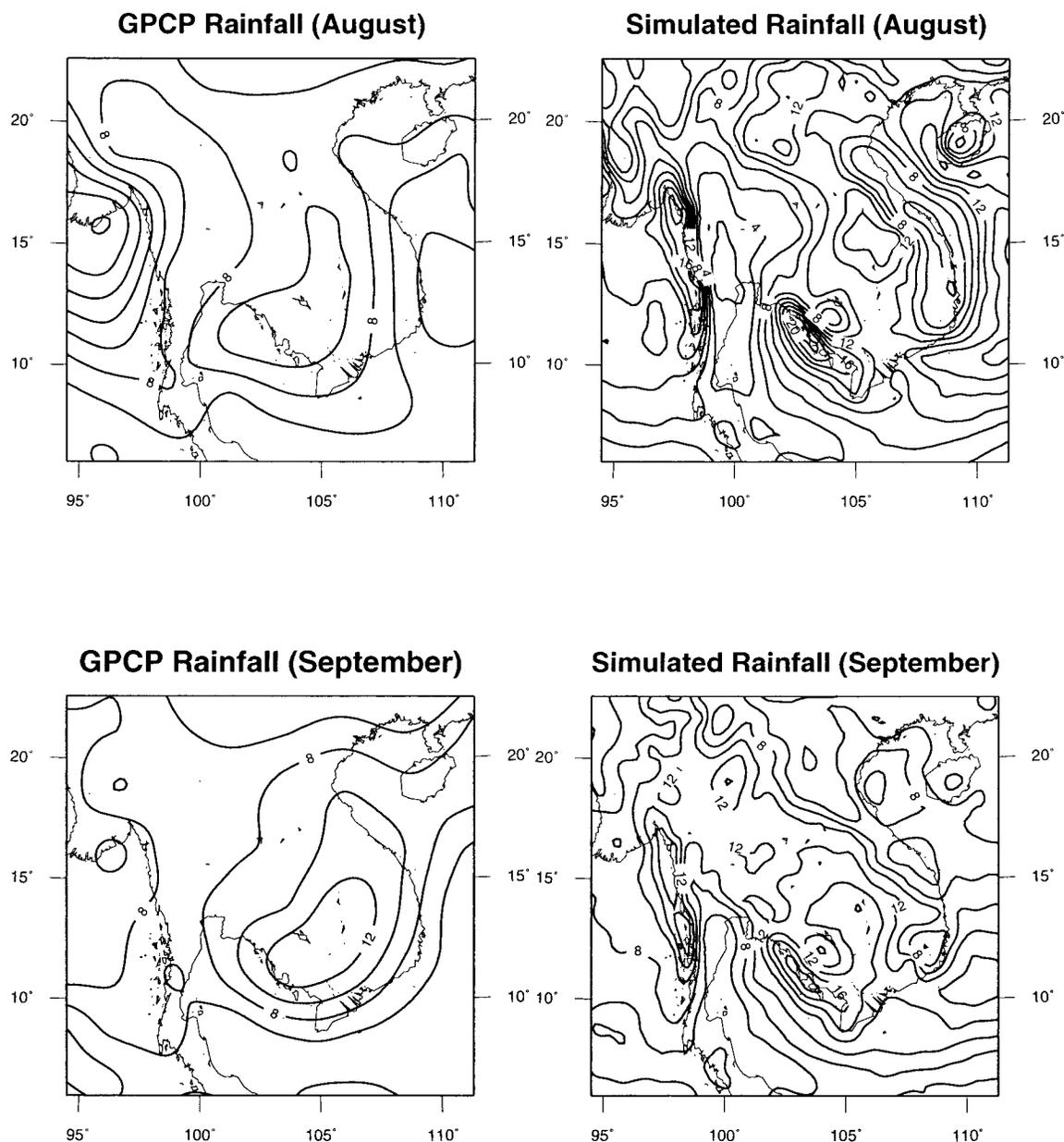## GPCP Rainfall (September)

Simulated Rainfall (September)

FIG. 12. Precipitation according to the (left) GPCP analysis and (right) simulated precipitation (CRRT) in (top) Aug and in (bottom) Sep. Contour interval is 2 mm day^{-1}.

lation, which should correspond to the decrease in observed precipitation. The maximum decrease in observed precipitation in September, measured at Nakhon Phanom station, is 173 mm month^{-1} (50 yr)$^{-1}$, which corresponds to 60% of the monthly mean precipitation at that station. The maximum decrease in simulated precipitation in September at a grid point within ALSC is 88 mm month^{-1}, which corresponds to 29% of the mean simulated precipitation at that grid point. The magnitude of the horizontally averaged decrease in precipitation all over ALSC in September is 26 mm month^{-1}. The simulated changes in precipitation are smaller than the

observed changes. This result is partly due to the fixed evaporation efficiency, which does not enhance a decrease or increase in precipitation through recycling of precipitation.

Changes in evaporation are shown in Fig. 14. A decrease in evaporation in August on the western and the eastern side of ALSC was obtained. The decrease is mostly less than 30 mm month^{-1}, and the horizontally averaged decrease over ALSC is 9 mm month^{-1}. In September, a decrease in evaporation over almost all of ALSC was obtained. The decrease in September is mostly less than 15 mm month^{-1}, and the horizontally av-

Aug. Precip.(CRRT-PAST)

Aug. Evapor.(CRRT-PAST)

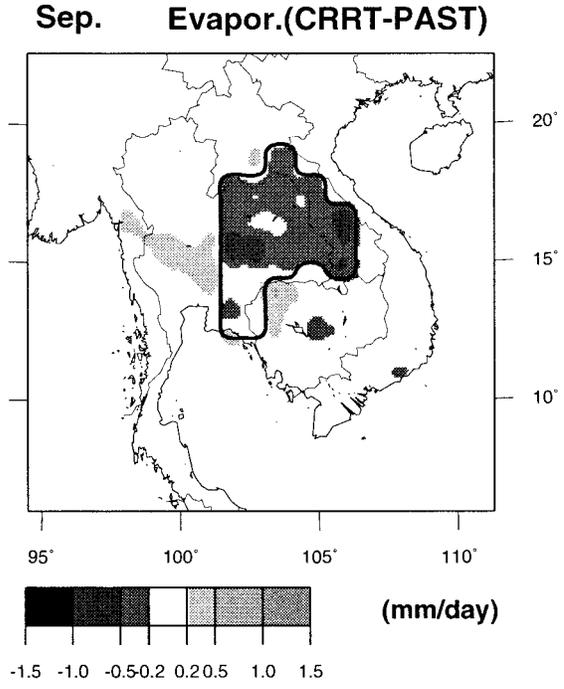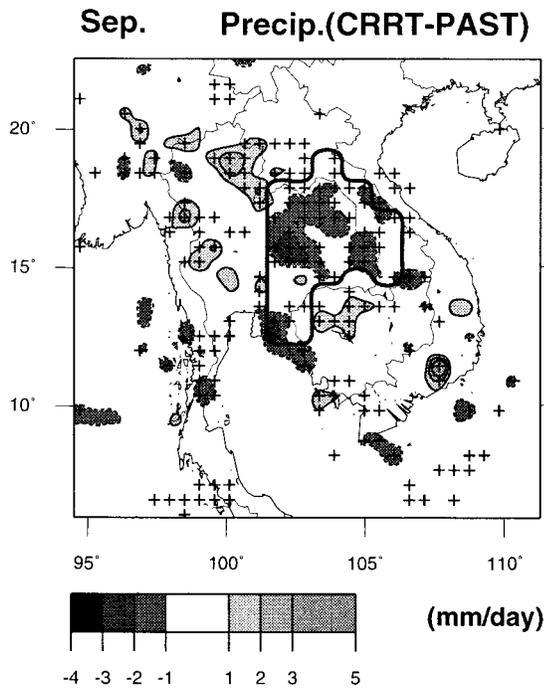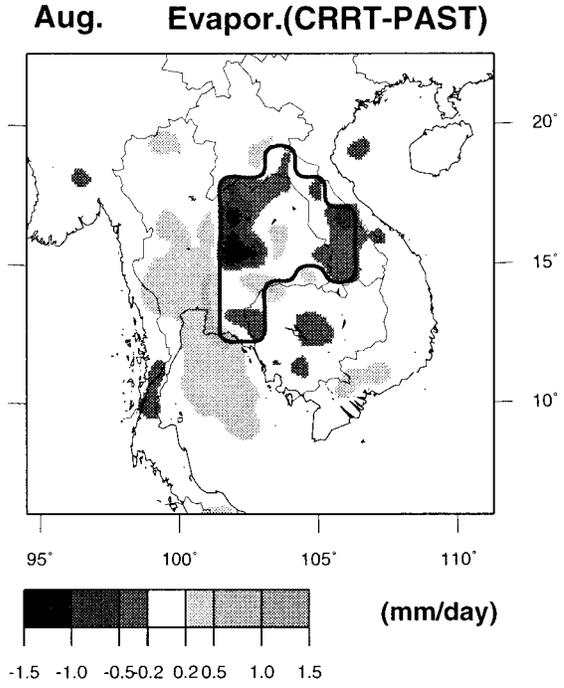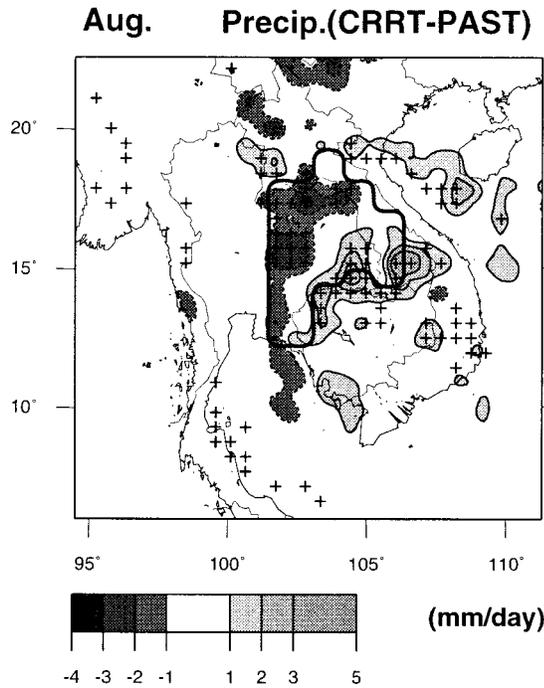## Sep. Precip.(CRRT-PAST)

Sep. Evapor.(CRRT-PAST)

FIG. 13. Change in simulated precipitation for (CRRT − PAST) in (top) Aug and (bottom) Sep. The cross mark in this figure denotes the grid points that are statistically significant at the 95% level as determined by the Student's t test.

FIG. 14. Change in simulated evaporation for (CRRT − PAST) in (top) Aug and (bottom) Sep.

eraged decrease over ALSC is also approximately 9 mm month⁻¹.

Surface air temperature over ALSC has increased by approximately 0.1–0.9°C. Surface specific humidity

over ALSC has decreased by less than approximately 5% at individual grid points.

The change in precipitation is likely to be related to the change in surface heat fluxes. Giorgi et al. (1996) described that there can be, in general, two opposite effects of land surface fluxes on precipitation. One is

that an increase in evaporation provides an additional moisture source for convection, which leads to an increase in precipitation. Another is that, on the other hand, a decrease in evaporation and an increase in sensible heat flux provide a source of buoyancy so that convective precipitation is enhanced.

Figure 15 shows a scattergram of the change in evaporation and the change in precipitation at each grid point in ALSC in August, and a scattergram of the change in sensible heat and the change in precipitation in August. In the figure, white circles denote values at the lateral boundary grid points within ALSC and black circles denote values on the rest within ALSC. Air masses at lateral boundary grid points within ALSC are likely to be affected by air masses from outside of ALSC. Thus, black circles might be more representative in terms of deforestation effects. The dotted line in the figure shows the points for which the decrease (increase) in precipitation is just the same as the decrease (increase) in evaporation. In Fig. 15, no relationship is apparent in the evaporation–precipitation scattergram or the sensible heat–precipitation scattergram.

Figure 16 shows the same scattergram but for September. In the upper panel of Fig. 16, the decrease in precipitation corresponds to the decrease in evaporation at many grid points in ALSC. The decrease in evaporation might cause the decrease in precipitation in September. The fact that the decrease in precipitation is mostly larger than the decrease in evaporation indicates a certain indirect effect of evaporation on precipitation (Schär et al. 1999). In the lower panel of Fig. 16, no clear relationship is evident.

Changes in some climate variables for (CRRT − VEGT) are addressed in the following. Figure 17 shows the change in precipitation. A decrease in the western part of ALSC and an increase in the eastern part of ALSC are evident in August. They could be more obvious if the contour intervals were smaller. In September, a decrease in precipitation over almost all of ALSC is evident. The magnitude of the decrease in precipitation in September is almost the same as in Fig. 13.

Scattergrams for (CRRT − VEGT) are presented in Figs. 18 and 19. In August (Fig. 18), no noteworthy characteristic is found in the analysis of the changes in precipitation. In September (Fig. 19), the decrease in precipitation corresponds to the decrease in evaporation at many points. The decrease in precipitation and the decrease in evaporation in September are distinct in (CRRT − VEGT) as well as in (CRRT − PAST). However, no linear relationship is seen between the change in evaporation and the change in precipitation.

On the whole, these characteristics of (CRRT − VEGT) in Figs. 18 and 19 seem to be similar to the characteristics shown in Figs. 15 and 16, though the absolute values in Figs. 18 and 19 are smaller than those in Figs. 15 and 16. The difference in the absolute values must be due to the difference in evaporation efficiency between PAST and VEGT.
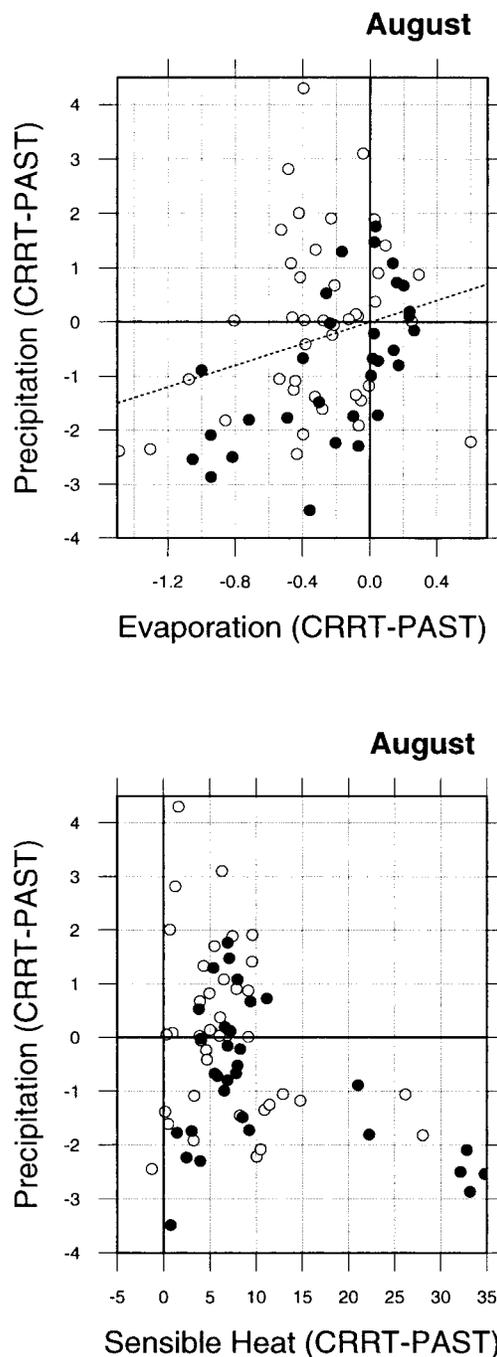

FIG. 15. (top) Scattergram of the change in evaporation (mm day^{-1}) and the change in precipitation (mm day^{-1}) for (CRRT − PAST) in Aug. (bottom) Scattergram of the change in sensible heat (W m^{-2}) and the change in precipitation (mm day^{-1}) for (CRRT − PAST) in Aug. The white circles denote the values at the lateral boundary grid points within the deforested area. The black circles denote the values at inner grid points.
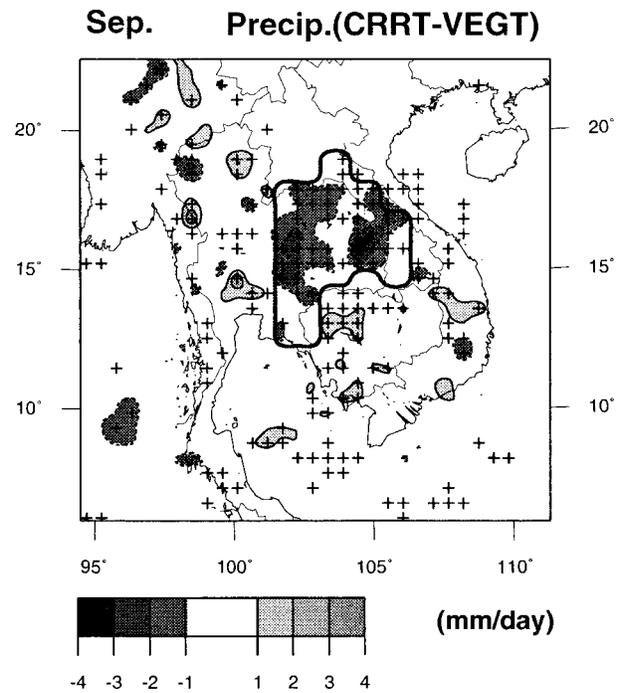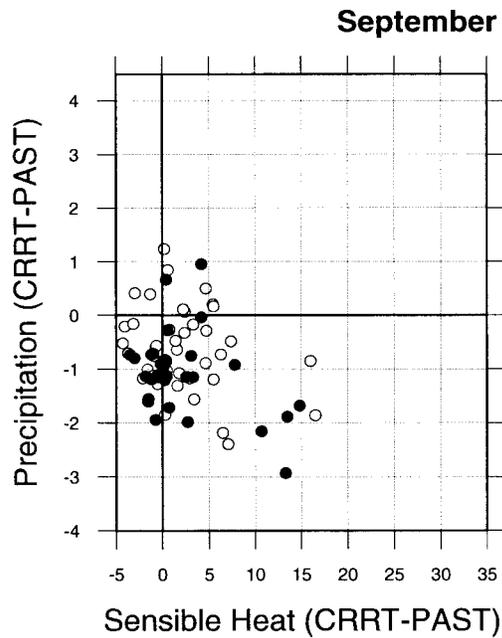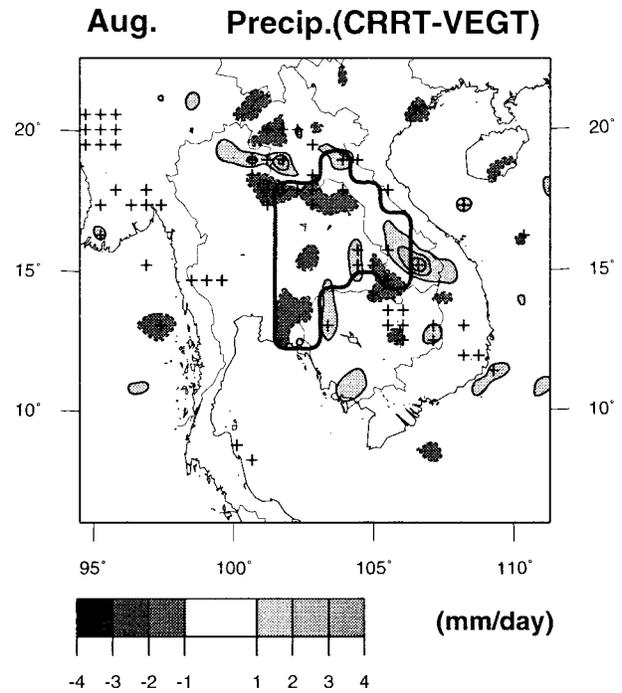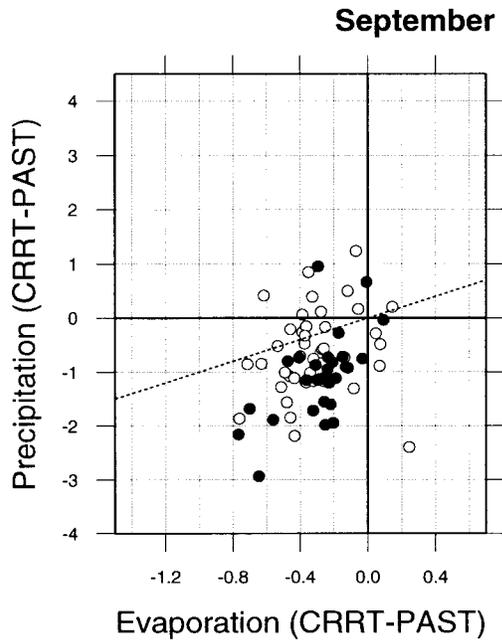
September

Aug.   Precip.(CRRT-VEGT)

September

FIG. 16. As in Fig. 15, but for Sep.

Sep.   Precip.(CRRT-VEGT)

FIG. 17. As in Fig. 13, but for (CRRT − VEGT).

Eltahir (1998) argued that the sum of evaporation and sensible heat flux (hereinafter, total heat flux) at the surface is an important parameter in the analysis of land surface–atmosphere interactions. The results of this study show no clear relationship between the change in total heat flux and the change in precipitation in August. In September, the relationship between the change in total heat flux and the change in precipitation is similar to that between the change in evaporation and the change in precipitation, because the change in sensible heat flux in September is small. It is impossible to distinguish between the evaporation–precipitation relationship and the total heat flux–precipitation relationship in September.
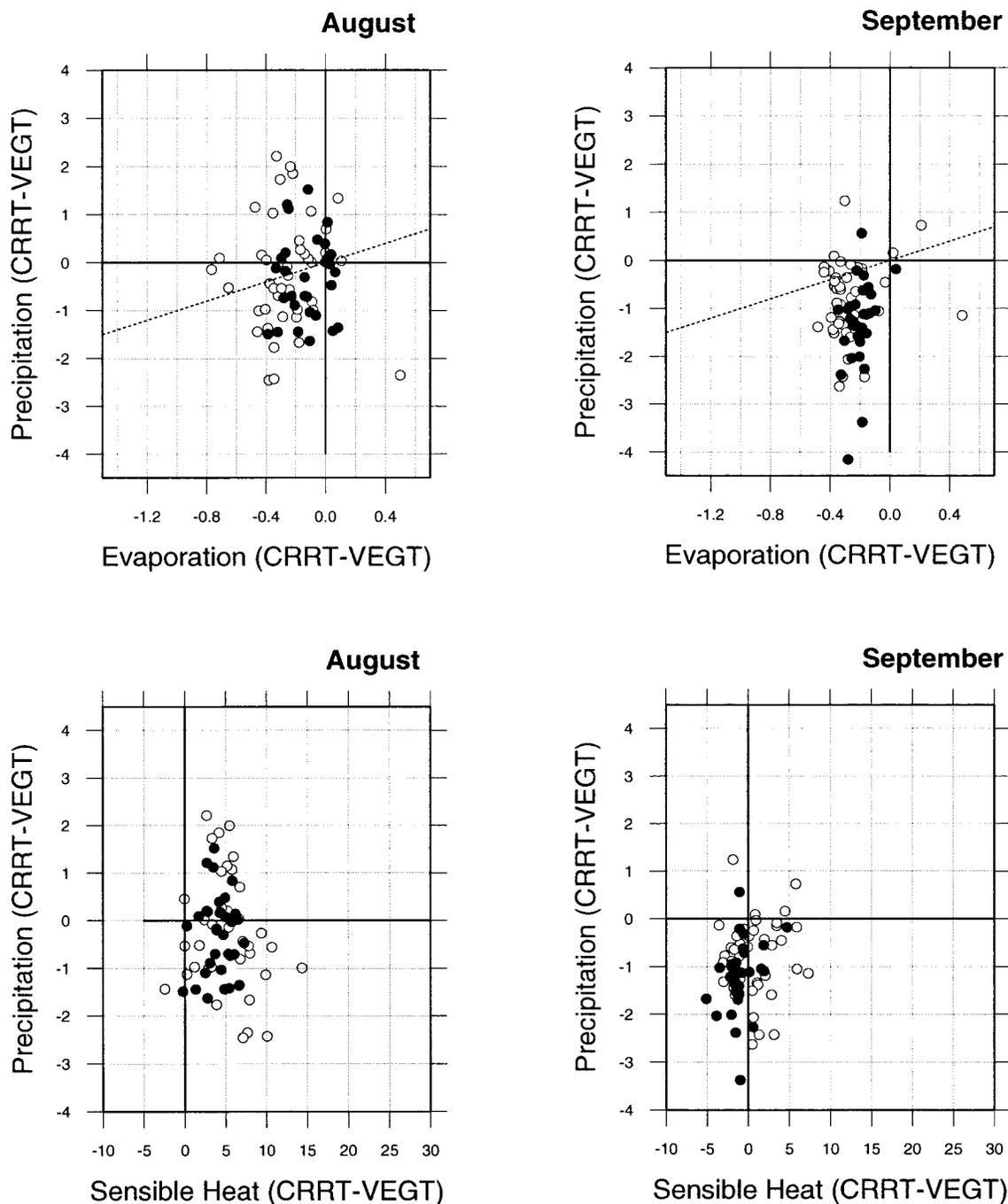
August

September

August

September

FIG. 18. As in Fig. 15, but for (CRRT − VEGT).

FIG. 19. As in Fig. 16, but for (CRRT − VEGT).

c. Mechanism

1) AUGUST

One explanation is given for the increase in precipitation in the eastern part of ALSC in August. The explanation below is based on the results of (CRRT − PAST). Figure 20 shows the change in horizontal water-vapor flux of (CRRT − PAST) at 950 hPa. A significant

change is clear only in August, and no distinct change is evident in September. The decrease in roughness length accompanied by the changes in vegetation enhanced the westerlies over ALSC in August, which caused the change in horizontal water vapor flux over ALSC. Hence, more water vapor in the atmosphere near the surface of CRRT was brought from the western part of ALSC to the eastern part as compared with the atmosphere of PAST. This must have caused the increase
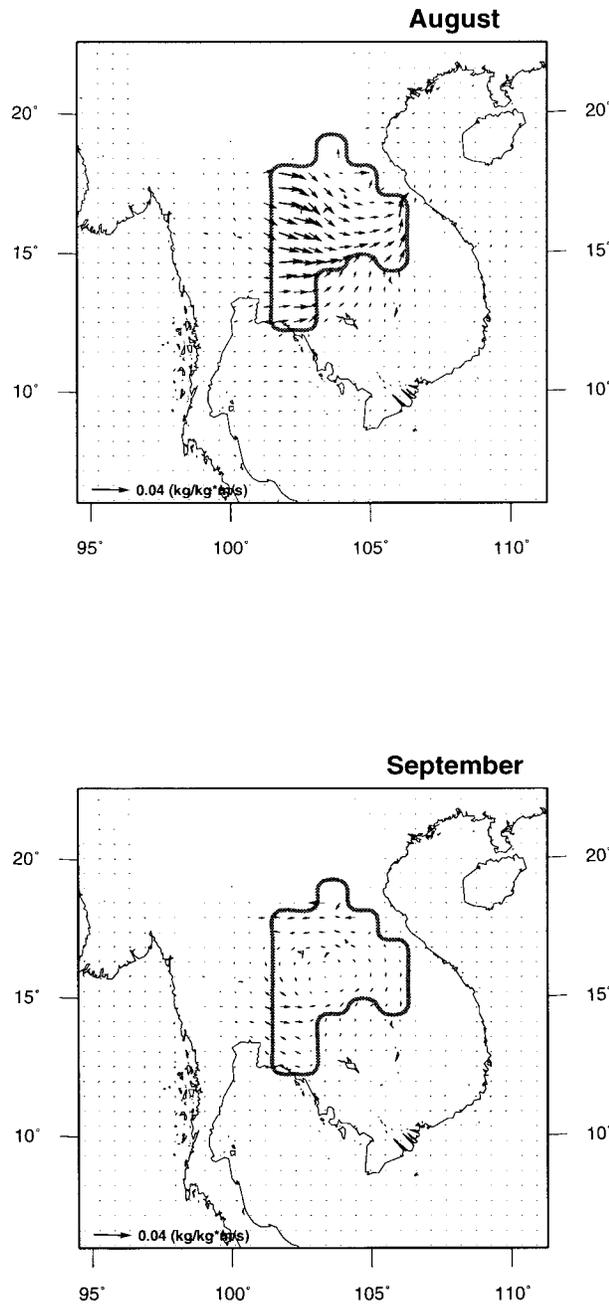
FIG. 20. Change in water vapor flux for (CRRT − PAST) at 950 hPa in (top) Aug and (bottom) Sep.

in precipitation in the eastern part. The chain of mountains located at the eastern end of ALSC, in Vietnam and Laos, must have played a role as a barrier that forces the convergence near the mountains and must have caused the increase in precipitation in the eastern part of ALSC. Such a strengthening of the dominant wind system near the surface was shown in the former Amazonian case (Lean and Rowntree 1997). They also argued that the high Andes barrier in their model must

have caused the forced convergence. The same characteristic of horizontal water-vapor flux described above can be seen in the results of (CRRT − VEGT).

2) SEPTEMBER

Although the decrease in evaporation may be one of the major causes of the decrease in precipitation in September, the fact that the decrease in precipitation was larger than the decrease in evaporation at many grid points in ALSC (in Figs. 16 and 19) indicates that the reduction in evaporation does not entirely account for the reduction in precipitation. There must exist a certain mechanism by which a change in a surface flux causes a change in precipitation.

Betts et al. (1996) proposed a theory based on a "land surface flux–convection" relationship. Their proposed theory is as follows. Suppose evaporation from the surface decreases and the sensible heat flux increases. Then, the increased sensible heat flux enhances the boundary layer deepening in the afternoon, which is accompanied by the enhancement of the entrainment at the top of the boundary layer. Thus, equivalent potential temperature θ_e in the boundary layer becomes lower because of the enhanced entrainment of lower θ_e at the top of the boundary layer. This decrease in θ_e causes the decrease in convective instability, because θ_e and θ_{es} (saturated θ_e) in the lower troposphere are the key parameters for convective instability. Therefore, Betts et al. (1996) argued that increased sensible heat flux and decreased evaporation from the surface reduce convective activity, even if the total heat flux is unchanged. This mechanism seemed to appear in the results of several numerical experiments (e.g., Beljaars et al. 1996; Schär et al. 1999).

Eltahir (1998) proposed a similar theory, but the importance of the magnitude of the total heat flux from the surface was emphasized rather than the magnitude of the entrainment at the top of the boundary layer. In the theory, it was insisted that the increase in the total heat flux from the surface is responsible for the increase in moist static energy per unit mass of air in the boundary layer. (Moist static energy and θ_e have an equivalent meaning in this context.) Because both theories argued on the importance of boundary layer θ_e (or moist static energy), θ_e of the boundary layer in this simulation is discussed below.

Figure 21 shows mean vertical profiles in θ_e and θ_{es} in the afternoon in September at grid points in ALSC at which the decrease in precipitation exceeds the decrease in evaporation. Such grid points represent 70% of ALSC. The decrease in θ_e described above is expected to be found. However, only a little difference can be seen between θ_e from CRRT and θ_e from PAST. On the other hand, a larger change is detected between θ_{es} from CRRT) and θ_{es} from PAST. The larger distance between θ_e and θ_{es} for CRRT, as compared with PAST, indicates a decrease in convective instability. The change in con-
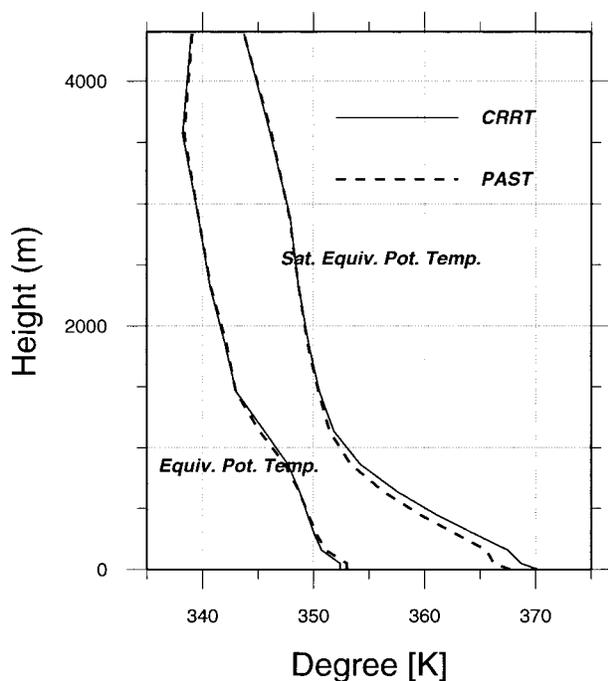
FIG. 21. Vertical profiles of (saturated) equivalent potential temperature in the afternoon in Sep for CRRT and PAST at the grid points for which the decrease in precipitation exceeds the decrease in evaporation within ALSC. These grid points represent 70% of ALSC.

vective instability is represented by the change in the vertical profile of θ_{es} in this case. The change in convective instability does not correspond to the change in θ_e as Betts et al. (1996) or Eltahir (1998) proposed.

The decrease in precipitation in the western part of ALSC in August is due to the same mechanism as in September, described above.

6. Discussion and conclusions

Precipitation records from 1951 to 1994 in Thailand were examined to detect the impact of tropical deforestation over the Indochina Peninsula. Analysis based on the monthly precipitation data revealed a distinct decrease in precipitation in September, which is approximately 100 mm month^{-1} and approximately corresponds to a relative change of 30% over the past three or four decades. A large increase in precipitation at the northeastern edge of Thailand was also found in July and August.

Numerical experiments with a regional climate model based on RAMS were carried out for August and September to examine the characteristics found in the observational analysis. Because a simple land surface scheme was utilized, albedo, roughness length, and evaporation efficiency over a part of Thailand (ALSC) were altered in between the numerical experiments.

A decrease in precipitation in the western part of

ALSC and an increase in precipitation in and near the eastern part of ALSC were evident in August in the results of the numerical experiments. A significant decrease in precipitation appeared over almost all of ALSC in September. One could argue that the increase in observed precipitation in the northeastern part of Thailand in August is qualitatively reproduced by the numerical experiments. In addition, the results suggest that the decrease in observed precipitation over Thailand in September is also qualitatively reproduced. The magnitude of the change in simulated precipitation is, however, smaller than the magnitude of the observed change.

To answer the question "Why does the significant decrease occur only in September?" the climate over the Indochina Peninsula is examined. Its most evident characteristic in September, in terms of the wind system, is the weak monsoon. Because the monsoon westerlies bring abundant moisture from the sea to the Indochina Peninsula until the end of August or the beginning of September, the effects of local land surface–atmosphere interactions should be weak in August. The local effect should be flushed away by the strong westerlies. This result means that the Indochina Peninsula can be defined as a maritime land until the end of August. On the other hand, the effects of local land surface–atmosphere interactions can be substantial in September when the monsoon winds disappear. The continuous deforestation through the last several decades probably has had a significant effect, resulting in a decrease in precipitation in September.

Thus, anthropogenic land surface changes can influence regional precipitation. A significant decrease in precipitation can appear in a specific period when advection is not dominant. It is also inferred that local precipitation–evaporation recycling might play a more important role in September than in other periods of the year. In addition, deforestation might have had an effect, resulting in an increase in precipitation at the northeastern edge of Thailand in August, mainly due to changes in roughness length.

In the previous studies on the Amazonian deforestation, such a decrease in precipitation has been discussed as a phenomenon occurring almost throughout the year or throughout the wet season and has not been discussed as a phenomenon occurring in a specific period of the year. Because the effect of land surface on precipitation over the Indochina Peninsula differs between two consecutive months in the wet season, it is suggested that the analysis of the effect of the land surface on the regional climate should be carried out by carefully considering the climatic characteristics for each period of the year.

In this study, the locations of the changes in precipitation obtained in the simulation did not necessarily coincide with the locations of the observed changes. This discrepancy in terms of the locations may be improved if more realistic distributions of land surface parameters both in the past and at present are used in

the experiments. The discrepancy between the magnitudes of the observed precipitation changes and those obtained in the experiments may be partly due to the fixed evaporation efficiency, which does not enhance a change in precipitation through recycling of precipitation.

Albedo and roughness length were the parameters primarily considered in the assessment of the physical effect of deforestation on precipitation in this study. However, a more sophisticated land surface scheme with additional vegetation parameters is expected to be used in future research. Numerical experiments using a more sophisticated land surface scheme will be useful for more realistic analysis of the complex behavior of hydrological and biological components at the land surface.

We have conducted a further series of numerical experiments on deforestation with coarser grid spacing and a larger domain (120 km; 60×45 grid points) to assess the effect of changing the size of the model domain. The settings in these experiments were similar to CRRT and PAST, except for the grid system. The results of this set of experiments were almost the same as those derived from CRRT and PAST. Therefore, the size of the model domain has little effect on the results of this study.

REFERENCES

Arakawa, A., and W. H. Schubert, 1974: Interactions of cumulus cloud ensemble with the large-scale environment. Part I. *J. Atmos. Sci.,* **31,** 671–701.

Arbhabhirama, A., D. Phantumvanit, J. Elkington, and P. Ingkasuwan, 1988: *Thailand: Natural Resources Profile.* Oxford University Press, 431 pp.

Beljaars, A. C. M., P. Viterbo, M. J. Miller, and A. K. Betts, 1996: The anomalous rainfall over the United States during July 1993: Sensitivity to land surface parameterization and soil moisture anomalies. *Mon. Wea. Rev.,* **124,** 362–383.

Betts, A. K., J. H. Ball, A. C. M. Beljaars, M. J. Miller, and P. A. Viterbo, 1996: The land surface–atmosphere interaction: A review based on observational and global modeling perspectives. *J. Geophys. Res.,* **101,** 7209–7225.

Chase, T. N., R. A. Pielke, T. G. F. Kittel, R. Nemani, and S. W. Running, 1996: Sensitivity of a general circulation model to global changes in leaf area index. *J. Geophys. Res.,* **101,** 7393–7408.

Chu, P.-S., and J.-B. Wang, 1997: Recent climate change in the tropical western Pacific and Indian Ocean regions as detected by outgoing longwave radiation records. *J. Climate,* **10,** 636–646.

——, Z.-P. Yu, and S. Hasternath, 1994: Detecting climate change concurrent with deforestation in the Amazon basin: Which way has it gone? *Bull. Amer. Metor. Soc.,* **75,** 579–583.

Davies, H. C., 1976: A lateral boundary formulation for multi-level prediction models. *Quart. J. Roy. Meteor. Soc.,* **102,** 405–418.

Dickinson, R. E., and A. Henderson-Sellers, 1988: Modelling tropical deforestation: A study of GCM land-surface parameterizations. *Quart. J. Roy. Meteor. Soc.,* **114,** 439–462.

Dirmeyer, P. A., A. J. Dolman, and N. Sato, 1999: The pilot phase of the Global Soil Wetness Project. *Bull. Amer. Meteor. Soc.,* **80,** 851–878.

Eltahir, E. A. B., 1998: A soil moisture–rainfall feedback mechanism: 1. Theory and observations. *Water Resour. Res.,* **34,** 765–776.

Emori, S., 1998: The interaction of cumulus convection with soil moisture distribution: An idealized simulation. *J. Geophys. Res.,* **103** (D8), 8873–8884.

Gash, J. H. C., and C. A. Nobre, 1997: Climatic effects of Amazonian deforestation: Some results from ABRACOS. *Bull. Amer. Meteor. Soc.,* **78,** 823–830.

Giorgi, F., L. O. Mearns, C. Shields, and L. Mayer, 1996: A regional model study of the importance of local versus remote controls of the 1988 drought and the 1993 flood over the central United States. *J. Climate,* **9,** 1150–1162.

Hahmann, A. N., and R. E. Dickinson, 1997: RCCM2-BATS model over tropical South America: Applications to tropical deforestation. *J. Climate,* **10,** 1944–1964.

Henderson-Sellers, A., and V. Gornitz, 1984: Possible climatic impacts of land cover transformations, with particular emphasis on tropical deforestation. *Climatic Change,* **6,** 231–258.

——, R. E. Dickinson, T. B. Durbidge, P. J. Kennedy, and K. McGuffie, 1993: Tropical deforestation: Modeling local- to regional-scale climate change. *J. Geophys. Res.,* **98,** 7289–7315.

Huffman, G. J., and Coauthors, 1997: The Global Precipitation Climatology Project (GPCP) Combined Precipitation Data Set. *Bull. Amer. Meteor. Soc.,* **78,** 5–20.

Jha, R., S. Herath, and K. Musiake, 1998: Application of IIS distributed hydrological model (IISDHM) in Nakhon Sawan catchment, Thailand. *Annu. J. Hydraul. Eng., JSCE,* **42,** 145–150.

Kalnay, E., and Coauthors, 1996: The NCEP/NCAR 40-Year Reanalysis Project. *Bull. Amer. Meteor. Soc.,* **77,** 437–471.

Khromov, S. P., 1957: Die geographische Verbreitung der Monsune (The geographical distribution of the monsoon). *Petermanns Geogr. Mitt.,* **101,** 234–237.

Kousky, V. E., and P.-S. Chu, 1978: Fluctuations in annual rainfall for northeast Brazil. *J. Meteor. Soc. Japan,* **56,** 457–465.

Lean, J., and P. R. Rowntree, 1997: Understanding the sensitivity of a GCM simulation of Amazonian deforestation to the specification of vegetation and soil characteristics. *J. Climate,* **10,** 1216–1235.

Louis, J. F., 1979: A parametric model of vertical eddy fluxes in the atmosphere. *Bound.-Layer Meteor.,* **17,** 187–202.

Manabe, S., 1969: Climate and the ocean circulation, I. The atmospheric circulation and the hydrology of the earth's surface. *Mon. Wea. Rev.,* **97,** 739–774.

Matsumoto, J., 1995: Rainfall climatology over Asian monsoon region. *Toward Global Planning of Sustainable Use of the Earth,* S. Murai, Ed., Elsevier Science, 419–422.

Mellor, G. L., and T. Yamada, 1982: Development of a turbulence closure model for geophysical fluid problems. *Rev. Geophys. Atmos. Phys.,* **20,** 851–875.

Moorthi, S., and M. J. Suarez, 1992: Relaxed Arakawa–Schubert: A parameterization of moist convection for general circulation models. *Mon. Wea. Rev.,* **120,** 978–1002.

Murakami, T., and J. Matsumoto, 1994: Summer monsoon over the

Asian continent and western North Pacific. *J. Meteor. Soc. Japan,* **72** (5), 719–745.

Nakajima, T., and M. Tanaka, 1986: Matrix formulation for the transfer of solar radiation in a plane-parallel scattering atmosphere. *J. Quant. Spectrosc. Radiat. Transfer,* **35,** 13–21.

Oki, T., K. Musiake, H. Matsuyama, and K. Masuda, 1995: Global atmospheric water balance and runoff from large river basins. *Hydrol. Processes,* **9,** 655–678.

——, T. Nishimura, and P. Dirmeyer, 1999: Assessment of land surface models by runoff in major river basins of the globe using Total Runoff Integrating Pathways (TRIP). *J. Meteor. Soc. Japan,* **77,** 235–255.

Pielke, R. A., and Coauthors, 1992: A comprehensive meteorological modeling system—RAMS. *Meteor. Atmos. Phys.,* **49,** 69–91.

——, R. Avissar, M. Raupach, A. J. Dolman, X. Zeng, and A. S. Denning, 1998: Interactions between the atmosphere and terrestrial ecosystems: Influence on weather and climate. *Global Change Biol.,* **4,** 461–475.

——, R. L. Walko, L. T. Steyaert, P. L. Vidale, G. E. Liston, W. A. Lyons, and T. N. Chase, 1999: The influence of anthropogenic landscape changes on weather in south Florida. *Mon. Wea. Rev.,* **127,** 1663–1673.

Press, W. H., S. A. Teukolsky, W. T. Vetterling, and B. P. Flannery, 1992: *Numerical Recipes in C: The Art of Scientific Computing.* 2d ed. Cambridge University Press, 994 pp.

Reynolds, R. W., 1988: A real-time global sea surface temperature analysis. *J. Climate,* **1,** 75–86.

Royal Forest Department of Thailand, 1994: Forestry statistics of Thailand. Royal Forest Dept. of Thailand Report. [Available from Planning Division, Royal Forest Dept. of Thailand, Chatujak, Bangkok 10900, Thailand.]

Schär, C., D. Lüthi, U. Beyerle, and E. Heise, 1999: The soil–precipitation feedback: A process study with a regional climate model. *J. Climate,* **12,** 722–741.

Sellers, P. J., and Coauthors, 1995: *ISLSCP Initiative I—Global Data Sets for Land–Atmosphere Models, 1987–1988.* NASA, CD-ROM.

Sud, Y. C., R. Yang, and G. K. Walker, 1996: Impact of in situ deforestation in Amazonia on the regional climate: General circulation model simulation study. *J. Geophys. Res.,* **101,** 7095–7109.

Walko, R. L., W. R. Cotton, M. P. Meyers, and J. Y. Harrington, 1995: New RAMS cloud microphysics parameterization, Part I: The single-moment scheme. *Atmos. Res.,* **38** (1–4), 29–62.

Watanabe, M., and M. Shinoda, 1996: Long-term variability of Asian summer monsoon rainfall during 1946–1988. *J. Meteor. Soc. Japan,* **74** (6), 923–934.

Xue, Y., and J. Shukla, 1993: A numerical experiment to study the influence of changes in the land surface properties on Sahel climate. Part I: Desertification. *J. Climate,* **6,** 2232–2245.

Zheng, X., and E. A. B. Eltahir, 1998: The role of vegetation in the dynamics of West African monsoons. *J. Climate,* **11,** 2078–2096.